

Giant conductance and phase time anomalous events of hole quantum transport.

S. Arias-Laso^a, L. Diago-Cisneros^b

^a*Departamento de Física, ISPJAE, C.P. 19390, La Habana, Cuba.*

^b*Departamento de Física Aplicada, Facultad de Física, Universidad de La Habana, C.P.10400, Cuba.*

Abstract

Events of giant conductance and anomalies of the phase transmission time for holes, are theoretically investigated within the multicomponent scattering approach. Based on this model, new analytical expressions for unitarity relations in the uncoupled hole transport are obtained and directly applied to study the behavior of the conductance and the phase transmission time in a double barrier resonant tunneling (DBRT) and a superlattice $GaAs$ -cladding layer/ $(AlAs/GaAs)^n/GaAs$ -cladding layer. Clear-signature evidences of giant conductance phenomena for hole transmission without valence-band mixing through a DBRT and a superlattice were found. The giant conductance effect losses robustness by manipulating the number of superlattice layers and by including the valence-band particles coupling as well. Phase time through the heterostructure exhibits extremal dependencies in the gaps and in the barriers, as those reported before for electrons. We have detected an earlier arrival phase time for the propagation of both flavors of holes within the barrier, in the order of few tenths of picoseconds. An appealing filter-like effect is presented, whenever a selective confinement strength arises independently for both flavors of holes in the uncoupled regime. Our results also prescribe noticeable evidences for both uncoupled and coupled hole fluxes, similar to those foretold by Hartman, upon transmission of electrons through opaque barriers.

Keywords: tunneling, phase time, elastic quantum scattering

PACS: 73.43.Jn, 34.80.Bm

1. Introduction

The impressive development of low-dimensional electronic and optoelectronic devices, brought a new urgency to the essential measurement and modeling of charge carriers transmission time and particularly of the tunneling time through specific potential regions. When electrons and holes are involved, the low-dimensional device response depends on the slower charge-carrier's traveling time [1]. Undoubtedly, for such systems it is crucial to study the tunneling time of holes. An equally important reason for address investigations on heavy holes (hh) and light holes (lh), is their intrinsic band mixing effects. Since the hole's transport is essentially an interconnected-multichannel process, the theoretical calculation of transmission quantities is in some sense more cumbersome than that for electrons.

Currently, the research of under-synchronic anomalous scattering events, is one of the major areas in the quantum transport theory[2–7]. Regarding the long-standing controversy around superluminal velocities and total transmission inconsistency, together with their wide-known anomalous character [8, 9], they are welcome due to all possible benefits they open up for design and development of nano-optoelectronic devices[2, 12, 13]. There is a large accumulated knowledge about these topics -mostly dedicated

to electrons, optical pulses and electromagnetic waves [5, 10–15]-, accurately enough to unambiguously provide solid grounds for superluminal propagation, the paradoxical Hartman premonition and legitimacy of the phase time approach. Worthwhile noticing however that, hole transport analogous phenomena has been less studied yet.

Resonant mechanisms between propagating modes oscillations and the self oscillations of the system are the fundamental cause, which gives rise to an isolated maximums of transmission, often referred to as giant conductance (GG) phenomena. Events of GG have been observed for electrons and optical pulses in many finite periodic systems, which possess time reversal symmetry, namely: ballistic mesoscopic conductors, luminal pulses and superlattices [17, 19–22]. Recent theoretical studies in molecular devices suggested that could rise up particularly large values for dynamic conductance [23] and novel experimental achievements pointed out to a giant enhancement of electronic tunneling in a two-dimensional lattice of graphene[24, 25]. Lately, was found a strong dependence of the conductance fluctuations with the density of states in graphene nanoribbons, which represent an alternative insight to study the band structure of these physical systems[26].

Owing to its relevance for quantum transport, the tunneling time has played a key role for a correct evaluation of electronic devices [8]. A large number of proposals in reply the challenge to settle how long does it takes to a

Email addresses: sariaslaso@gmail.com (S. Arias-Laso),
ldiago@fisica.uh.cu (L. Diago-Cisneros)

particle to tunnel a single potential barrier [30], have been put forward [8, 9, 34]. The lively and long standing debate concerning this matter [8, 9, 28, 30–35] –presumed not to finish completely–, it seems to have finally found its cornerstone in precise experimental measurements for photons and optical pulses [12, 13, 36–38]. These genuine measurements put to the test, before all else, the very question loosely formulated by McColl and directly bear on truly temporal features of tunneling phenomenon. Besides, they are consistent with the phase time conception derived from group delay within the stationary-phase method [28, 29, 31]. An additional motivation was the accurate description of above mentioned experiments by careful phase-time calculations [10, 11].

In this paper we will present numerical calculations of the conductance and the phase time for an arbitrary number of alternate layers of $III-V$ materials, in the framework of the multicomponent scattering approach (MSA)[3]. The main idea is to search evidences of anomalous events in hh and lh transmission. In Sec.2 some theoretical remarks within the MSA are exposed. Brief complementary insights to the uncoupled regime formula of scattering matrix unitarity relations and phase time will also be presented. Analytical expressions for the phase time and the conductance are applied in Sec.3 to study the anomalous events associated with these physical quantities in the double barrier resonant tunneling (DBRT) and the superlattice. Phase time behavior for holes shows a very good agreement with the previous results for electron-tunneling through superlattices[11]. Evidences of the giant conductance phenomena for uncoupled hole transport are shown. Finally, in Sec.4 we summarize and conclude.

2. Conduction and phase time in the multicomponent scattering approach

The MSA is based on standard $(N \times N)$ $\mathbf{k} \cdot \mathbf{p}$ effective Hamiltonians and the multichannel transfer matrix (TM) method. In this approach the scattering amplitudes can be obtained straightforwardly [3]. The main purpose here, is to evaluate quantities of synchronic multi-mode transport for massive charge carriers moving through multi-layered structures at coupled and decoupled channel regimes.

Owing to consistency, we found useful to recall few basic outlines of the Kohn-Luttinger (KL) two-band model [39], due to its widely accepted accuracy for describing dynamics of elementary excitations as well as electronic properties in the valence band, within the framework of the multiband effective mass approach. This model, is highly common regarding to the field of hole quantum transport through periodic heterostructures. It considers in the $\mathbf{k} \cdot \mathbf{p}$ approximation the highest two valence bands degenerated in the Γ -point of the Brillouin Zone. The usual (4×4) KL Hamiltonian [39] in the Broide-Sham representation

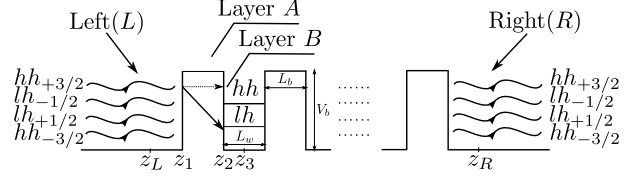


Figure 1: Schematic illustration of multichannel hh and lh quantum transport processes through a $GaAs$ – cladding layer(L)/($AlAs/GaAs$)ⁿ/ $GaAs$ – cladding layer(R) superlattice.

[3], has the form

$$\hat{H}_{KL} = \begin{pmatrix} H_{11} & H_{12} & H_{13} & 0 \\ H_{12}^* & H_{22} & 0 & -H_{13} \\ H_{13}^* & 0 & H_{22} & H_{12} \\ 0 & -H_{13}^* & H_{12}^* & H_{11} \end{pmatrix}, \quad (1)$$

with

$$\begin{aligned} H_{11} &= A_1 \kappa_T^2 + V(z) - B_2 \frac{\partial^2}{\partial z^2}, \\ H_{12} &= \frac{\hbar^2 \sqrt{3}}{2 m_0} (\gamma_2 (k_y^2 - k_x^2) + 2i \gamma_3 k_x k_y), \\ H_{13} &= i \frac{\hbar^2 \sqrt{3}}{2 m_0} \gamma_3 (k_x - i k_y) \frac{\partial}{\partial z}, \\ H_{22} &= A_2 \kappa_T^2 + V(z) - B_1 \frac{\partial^2}{\partial z^2}, \end{aligned}$$

being

$$\begin{aligned} A_{1,2} &= (\gamma_1 \pm \gamma_2) \\ B_{1,2} &= (\gamma_1 \pm 2\gamma_2), \end{aligned}$$

in atomic units. The matrix elements H_{ij} show a direct dependency of the semi-empirical parameters of Luttinger γ_i ($i = 1, 2, 3$), that typify each slab of the heterostructure. While $V(z)$ and κ_T , stand for the periodic potential, and the two-components in-plane *quasi*-momentum, respectively [3].

To study the quantum transport properties of holes through semiconductor heterostructure, we consider the system shown in Fig.(1), described by the Kohn-Luttinger Hamiltonian in the expression (1). The four accessible channels of the system, denoted as: *channel 1* : $hh_{+3/2}$, *channel 2* : $lh_{-1/2}$, *channel 3* : $lh_{+1/2}$, and *channel 4* : $hh_{-3/2}$, are considered simultaneously, following one of the bare bones of the MSA. We emphasize this upmost advantage, as it allows clearly identify inter- and intra-subband hole transitions together with transitions from Kramer-up toward Kramer-down states to time reversal, and the other way around. The latter is not the usual case. In this approach, the segment between z_L and z_3 in Fig. (1), is defined as a *cell* and represents the period of the heterostructure superlattice [3].

Combining the (4×4) Kohn-Luttinger Hamiltonian with the TM formalism, a direct connection with the scattering theory is established [3], then we have $\mathbf{M}_{sv}(z_R, z_L) =$

$\mathcal{N}^{-1}\mathbf{M}_{fd}(z_R, z_L)\mathcal{N}$. Here, \mathcal{N} defines a relation between the traveling wave vectors of the tunneling problem and their derivatives, with the N -dimensional state vectors that describe a propagating or evanescent mode. This crucial transformation of the MSA, connects two different kinds of TM. The first class of TM, $\mathbf{M}_{fd}(z_R, z_L)$, relates the linearly independent state functions and their derivatives (fd) between two points of the heterostructure in the form $\mathbf{M}_{fd}(z_R, z_L) = \mathbf{N}(z_R) \cdot \mathbf{N}(z_L)^{-1}$, where the matrix $\mathbf{N}(z_i)$ can be constructed once the linearly independent solutions are obtained [40]. The second kind of TM, $\mathbf{M}_{sv}(z_R, z_L)$, whose elements describe a propagating or evanescent mode depending on the energy, connects the state vectors (sv) in two different points of the system. The mathematical structure of these two matrices is conditioned by requirements of time-reversal invariance and flux conservation [41]. A very strong criterium to verify the calculations is based in the determinant of these transfer matrices which must be constant and equal to the unity, mostly.

Then applying the well known relations between the $\mathbf{M}_{sv} = \begin{pmatrix} \alpha & \beta \\ \gamma & \delta \end{pmatrix}$, and the scattering matrix $\mathbf{S} = \begin{pmatrix} r & t' \\ t & r' \end{pmatrix}$ blocks [41], one can directly evaluate the relevant physical quantities of the scattered transport theory. Initially we have to obtain the complex transmission amplitudes [3]

$$\begin{aligned} t &= \alpha - \beta\delta^{-1}\gamma, \\ t_{ij} &= t_{R_{ij}} + it_{I_{ij}}, \end{aligned} \quad (2)$$

for each transition from the j -th incoming channel (incident propagating mode) to the i -th outgoing channel (transmitted or reflected propagating modes). It is worth noticing that within the MSA, none of the incoming amplitudes is required to cancel, as it is commonly done. Hence, an authentic multichannel and synchronic description of the hole transmission processes is naturally achieved. This is to say that, we are able to distinguish accurately the contribution from each input channel to the scattering process, modulated by the simultaneous presence of the rest of the channels, which are, in principle, equally accessible to the incident hole stream. None of the usual simplifications of the original $\mathbf{k} \cdot \mathbf{p}$ Hamiltonians are invoked, thus the time reversal symmetry is assured. Given the transmission amplitudes t_{ij} , it is possible to evaluate the total transmission probability to channel i

$$G_i = (e^2/\pi\hbar) \sum_j |t_{ij}|^2, \quad (3)$$

the total two-probe Landauer conductance defined as [3, 42]

$$G = (e^2/\pi\hbar) \sum_{i,j} |t_{ij}|^2, \quad (4)$$

and the transmission amplitude phase for each of the 16 available paths ij [3], $\theta_{ij} = \arctan\{t_{I_{ij}}/t_{R_{ij}}\}$. The trans-

mission phase time is obtained from [3]

$$\tau_{ij} = \hbar \frac{\partial}{\partial E} \theta_{ij}, \quad (5)$$

whose advantages and applicability criteria has been widely discussed in the literature [3, 10, 11, 13, 43]. The sums in equations (3) and (4) run over all the open channels and the expressions (3)-(5) and (8) are defined for the n cells periodic structure showed in Fig.(1). Hereafter E stands for the incoming particle's energy.

Tunable parameter κ_T , is essential to modify the in-plane dynamics of holes, *i.e.* the degree of freedom transverse to the main transport direction, also refereed as the valence-band mixing for holes. This later is crucially relevant in order to understand the main problem envisioned here, and how we face it within the MSA. Whenever the *quasi*-momentum parallel to the interfaces, $\kappa_T \approx 0$, the crossed transitions are not allowed and the system is said to yield an uncoupled hole regime. Under this particular condition, only direct incoming-outgoing channels are connected, therefore (4×4) blocks α , β , γ and δ of the TM \mathbf{M}_{sv} are diagonal matrices. The later, straightforwardly leads us to new unitarity relationships, that satisfy the blocks of the multiband scattering matrix \mathbf{S} under an uncoupled hole regime, acquiring a more simple form:

$$\begin{aligned} \alpha^* \alpha - \beta^* \beta &= I_{N'} \\ \beta^* \delta - \gamma \alpha^* &= O_{N'} \\ \beta \delta^* - \gamma^* \alpha &= O_{N'} \\ \delta \delta^* - \gamma \gamma^* &= I_{N'}, \end{aligned} \quad (6)$$

where $N' = N/2$. Consequently, transmission and reflection amplitudes have reduced expressions respect to (2):

$$\begin{aligned} t &= 1/\alpha^* & \text{with } \alpha_{ii} &= \alpha_{R_{ii}} + i\alpha_{I_{ii}} \\ r &= -\delta^{-1}\gamma & \text{with } \delta(\gamma)_{ii} &= \delta(\gamma)_{R_{ii}} + i\delta(\gamma)_{I_{ii}} \end{aligned} \quad (7)$$

Rewriting the phase time (5) for this specific case, we obtain:

$$\tau_{ii} = \frac{\hbar}{T_{ii}} (\alpha_{R_{ii}} \frac{\partial \alpha_{I_{ii}}}{\partial E} - \alpha_{I_{ii}} \frac{\partial \alpha_{R_{ii}}}{\partial E}). \quad (8)$$

Expressions like (7) were previously reported for the resonant tunneling and band mixing in multichannel superlattices of propagating electron systems [11].

3. Numerical results and discussion: tunneling time and giant conductance

For the numerical calculations that will be presented here we shall consider our layered media with barrier thickness $L_b = (10 - 180) \text{ \AA}$, and well width $L_w = (50, 150) \text{ \AA}$. For the barrier height we will have either $V_b = 0.498 \text{ eV}$ or $V_b = 0.550 \text{ eV}$. The cases where the in-plane wavenumber (parallel to the interfaces) $\kappa_T \approx 0$, with vanishing band mixing effects, and the cases where $\kappa_T \neq 0$, with coupling phenomena effects on the quantum transport [3, 44, 45] will be separately study. Focusing to study the behavior of the

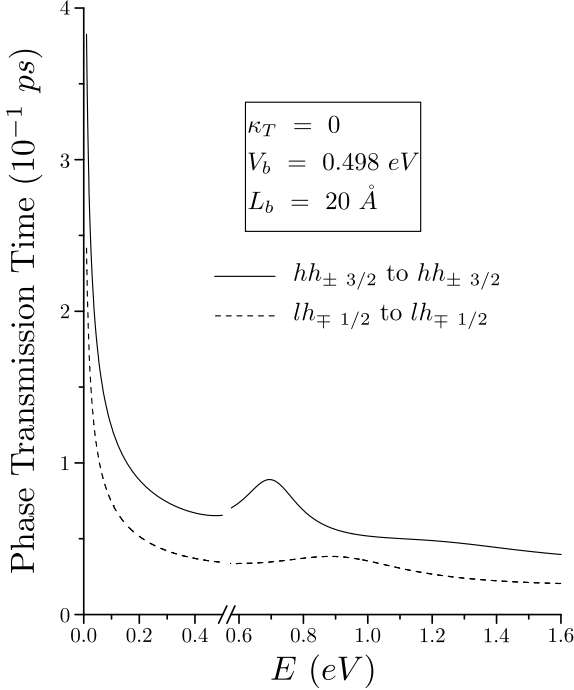


Figure 2: Phase time τ_{ii} for a tunneling of holes through a single barrier of $L_b = 20 \text{ \AA}$, as a function of the hole incident energy at $\kappa_T = 0$ with $V_b = 0.498 \text{ eV}$. The solid (dashed) line stands for $i = hh_{+3/2} (lh_{-1/2})$ direct path. In the broken interval a negative dip extends up to 0.4 ps .

phase time τ_{ii} and the free motion time $\tau_f = nl_c m_h^* / \hbar (k_z)_h$ (being l_c the cell longitude, m_h^* the effective mass of holes and $(k_z)_h$ the eigenvalues of the scattering problem solved with the MSA[3]) as a function of the incoming energy E_i , the barriers height and thickness were fixed at $V_b = 0.23 \text{ eV}$ and $L_b = 30 \text{ \AA}$, respectively. Both, a double barrier ($n = 2$ cells) and a superlattice of $n = 8$ cells were considered. For consistency with the reported results for electrons[11], a 30% concentration of *Al* was fixed inside the barrier: $(GaAs/Al_{0.3}Ga_{0.7}As/GaAs)^n$.

3.1. Uncoupled hole regime phenomena

In Figure 2, we plot the phase time for *lh* and *hh* through a single potential barrier. It is clear from this figure that the *lh* modes (dashed line) are faster than *hh* modes (solid line), although the difference is not large. In an effort to validate our numerical simulation with experimental data, we compare the results of Figure 2 with those of Dragoman *et. al.* [2] The tunneling times measured for holes, for null or small magnetic field in a ballistic-regimen nano-device, are of the order of 10^{-13} s . To reproduce that situation, we canceled the interaction between holes by assuming $\kappa_T \approx 0$ (uncoupled regimen), in the absence of magnetic field. In our calculation the phase time for *hh* and *lh* is also of the order of 10^{-13} s , which is in an acceptable qualitative agreement with experiment and it is just one order less than the traveling time for electrons through a single barrier [46], as was detected experimentally for a DBRT [43]. We have observed broaden

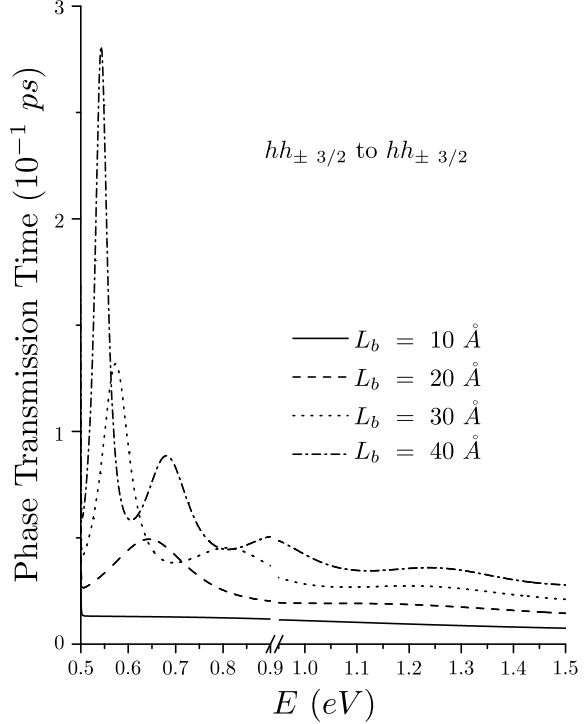


Figure 3: Direct phase time τ_{ii} for hole tunneling through a single barrier as a function of the hole incident energy for several values of the barrier thickness at $\kappa_T \approx 0$, with $V_b = 0.498 \text{ eV}$ and $i = 1$.

peaks of the phase time for $hh_{+3/2}$ direct transition at $E \approx 0.7 \text{ eV}$ and for $lh_{-1/2}$ direct transition at $E \approx 0.9 \text{ eV}$. We have observed, although not plotted, that the transmission coefficient maxima are located at comparable energies. It was shown in Ref.[11] that, the tunneling time follows the band structure. This feature of hole tunneling agrees also with calculations of Ref.[27], where a particular case of the envelope function approximation was used. Evaluating the tunneling times for energies in the range $0.40 \text{ eV} \leq E \leq 0.60 \text{ eV}$ we have found, although not shown, a reduction of τ_{ii} in 3 orders of magnitude with respect to that shown in Figure 2 when the in-plane momentum changes as $\Delta\kappa_T = 0.001 \text{ \AA}$. This behavior of τ_{ii} , was earlier detected in experiments for a hole passage through a slightly different system [48] -a double asymmetric quantum well (QW)-, and is considered to arise from valence subbands mixing [48].

Figure 3 displays a raising of the phase time while L_b increases in the case of uncoupled regime ($\kappa_T \approx 0$) of holes incidence. The same is achieved for light holes, although not shown in this figure. This behavior agrees qualitatively with the results of an experiment on time-resolved luminescence spectroscopy [43]. For $E > 0.4 \text{ eV}$, τ_{ii} is sensitive to the raising of L_b and it is shown an oscillating behavior of the transmission phase time as function of the incident energy. The resonances shift to smaller energies, increasing their intensities with L_b . It is assumed understood that, when the de Broglie wavelength of the hole propagating mode is a multiple of L_b , there is a resonance in the trans-

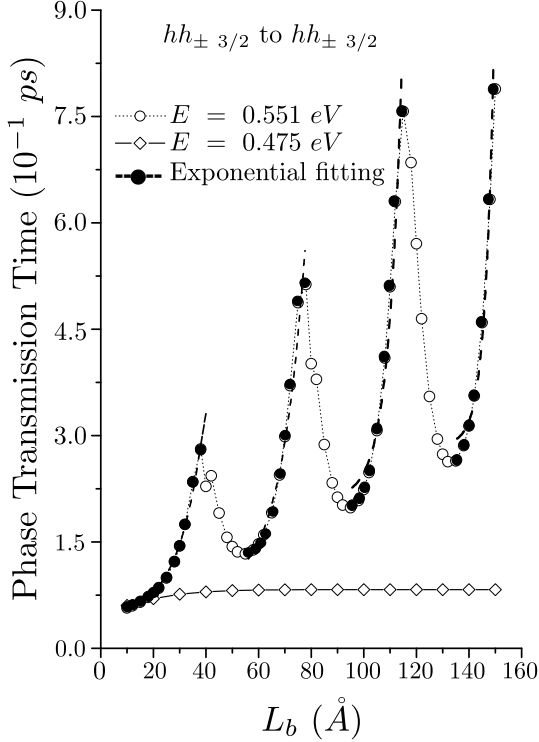


Figure 4: Phase time *versus* barrier thickness for the direct transitions $hh_{\pm 3/2} \rightarrow hh_{\pm 3/2}$ given as solid diamonds/circles ($E < V_b/E > V_b$), in the uncoupled case ($\kappa_T \approx 0$). A fragmented exponential fitting is shown in dashed line (with full circles) at $E = 0.551$ eV. The barrier height $V_b = 0.498$ eV.

mission and correspondingly the phase time delay raises at these energies. As L_b increases, new resonances appear, thus the oscillating behavior is achieved. These oscillations correspond to the quasi-stationary levels of the virtual QW with increasing width. In that sense, from τ_{ii} properties we are able to forecast a longer lifetime for the lower unbound hole levels. On general grounds, we found this in correspondence with the idea of the quasi-stationary states lowering, whenever the virtual QW becomes wider.

Figure 4 shows phase transmission time *versus* barrier thickness for the direct transitions $hh_{\pm 3/2} \rightarrow hh_{\pm 3/2}$ given as solid diamonds/circles ($E < V_b/E > V_b$), in the uncoupled case. We prescribe appealing tunneling events of holes for $E < V_b$ under uncoupled propagating regime. This figure displays τ_{ii} for resonant direct $hh_{\pm 3/2} \rightarrow hh_{\pm 3/2}$ transitions (diamonds), which rapidly becomes autonomous from barrier broadening as Hartman predicted for electrons [29]. These results are in accordance with the transit time for optical pulses through opaque barriers (which transmit about 10^{-4} of the incident radiation) [13] and also with theoretical predictions for the delay time in one and two dimensions [58]. The circles in Figure 4 correspond to numerical results within the MSA, for the tunneling time of direct paths (indicated in the legend) for $E > V_b$. Here we must stress, that the resonant oscillating behavior (on top of an average slope of smooth growth [59]), is an expected phenomena due to the barrier's inter-

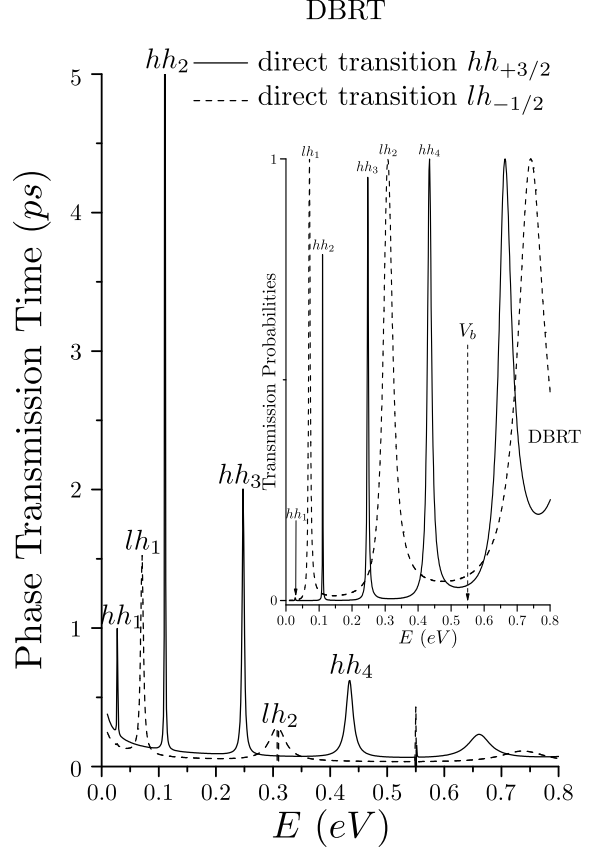


Figure 5: Direct phase time τ_{ii} for hole tunneling through a DBRT structure as a function of the energy of an impinging hole stream at $\kappa_T \approx 0$, with $V_b = 0.550$, $L_b = 20$ Å and $L_w = 50$ Å, for $i = hh_{+3/2}$ (solid line), and $i = lh_{-1/2}$ (dashed line). The inset displays transmission coefficients for the same direct transitions, through an identical DBRT heterostructure, as a function of the incident energy. The labelling for the hole levels follows that of the Reference [45].

ference effects with the continuum states, wide accepted as Ramsauer-Townsend oscillations [60]. For $E > V_b$ we briefly investigated segments in Figure 4, pursuing a locally exponential-like behavior of τ_{ii} , as was suggested in a reported experiment with holes [43], within a rank comparable with their measurements. The interval of barrier thickness length variance in their measurements, ranges from 30 Å up to 80 Å. Notice in Figure 4 a sectional fitting, using an exponential growth function [61] (dashed line with full circles). We do believe that oscillations are already intrinsically present in Heberle's, *et al.* accurate investigation [43] and could be shown by including more experimental points or enlarging in rank the search.

Phase time through DBRT and superlattice

Figure 5 is devoted to analyze briefly, the spectrum and the quasi-stationary bound states lifetime in a DBRT. The curves of Figure 5 (inset), show several transmission phase times τ_{ii} resonances for the uncoupled hole regime. In particular we have analyzed a semiconductor heterostructure of the form $GaAs/(AlAs/GaAs)^2/GaAs$. It was shown in Ref. [11] that the tunneling time follows the band struc-

Table 1: Comparison to typical quasi-steady DBRT hole-level structure with $V_b = 0,550$ eV, $L_b = 10$ Å, and $L_w = 50$ Å.

Levels [45]	Resonances [eV]	
	Experiment[53].	Theory (MSA).
hh_1	0,028	0,027
lh_1	0,073	0,071
hh_2	0,111	0,110
hh_3	0,245	0,247
lh_2	0,299	0,307
hh_4	0,428	0,434

ture profile. Figure 5 (inset) displays clearly, at $E < V_b$, the familiar discrete quasi-stationary hole-level spectrum of the embedded QW, widely accepted from hole quantum transport calculations [3, 27, 44, 49–52]. We have found at low energies ($E < V_b$), that the τ_{ii} resonances are allocated at energies which correctly reproduce the hole spectrum previously reported for the DBRT experiment [53], as expected (see Table 1). Notice the good quantitative agreement of our approach in Table 1, with similar values reported elsewhere [53]. A previous comparison [3] with a robust and widely accepted theoretical model [27], exhibits the advantages of the present approach.

Tunneling time can not be quantitatively determined from the resonant tunneling line width, [57] nevertheless some qualitative prognosis is allowed. Notice the general trend of larger values for hh states phase time in comparison to that of lh states. This is in correspondence with the properties we have found for the transmission-coefficient resonances depicted in the inset of Figure 5, which shows, as tendency, that hh resonances are thinner than the lh ones. This observation foretells a stronger confinement for heavy holes, and we guess it could be used in resonant-tunneling diode design and nano-modelling [45].

Among the different formulations of tunneling time with recurrent experimental agreement [34], the phase time have clearly advantages. In Reference [11], was demonstrated that the phase time associated with the passage (tunneling or not) of particles is a relevant quantity of the quantum transport, which was calculated and successfully compared with precise experimental measurements [12, 13]. Moreover in Reference [11], some appealing effects for electron phase time were predicted, namely: superluminal phase propagation and resonant-band structure. In an attempt to distinguish similar behaviors for holes, we perform some numerical simulations, exhibited in the next two figures.

In Figure 6 the phase transmission time $\tau_{1(2)}$, through a single cell ($n = 1$) and a DBRT ($n = 2$) respectively, together with T_2 are shown in connection with the free motion time τ_f (dotted line). The last, is the propagation time of the quasi-particle in absence of scattering potentials. The direct paths under analysis, are indicated in

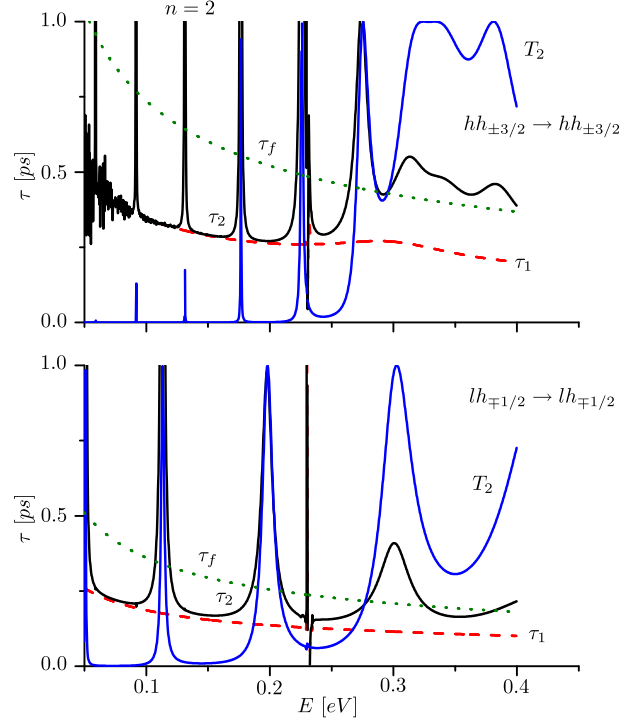


Figure 6: Top(Bottom) panel shows the evolution of the phase time, transmission probability, free motion time through $n = 2$ cells (DBRT) and the phase time through one single cell as function of the incoming energy for direct transitions of $hh_{\pm 3/2}$ ($lh_{\mp 1/2}$). With $V_b = 0.23$ eV, $L_b = 30$ Å and $L_w = 150$ Å. A 30% concentration of Al was fixed inside the barrier.

the legends of each panel. A resonant behavior for τ_2 is very clear for both hh states (top panel) and lh states (bottom panel). In the forbidden energy region, τ_2 approaches τ_1 (dashed red line), which represents its lower bound as had been foretold for electrons [11]. The relationship between τ_2 and T_2 (blue line) resonances - as one can see from (8)-, justify τ_2 to accurately reproduce, the quasi-stationary states of the embedded $GaAs$ QW. Another appealing feature arises for forbidden energy regions (T_2 vanishes), where $\tau_2 < \tau_f$. The opposite is predicted for allowed energies. For hh states (top panel) of incoming energies around 100 meV, $(\tau_f - \tau_2) \approx 0.4$ ps, while for lh states (bottom panel) $(\tau_f - \tau_2) \approx 0.1$ ps. This earlier arrival time for hh and lh , was predicted for electron tunneling through a same heterostructure [11], and suggest a more speedily passage of holes through a DBRT like $(GaAs/Al_{0.3}Ga_{0.7}As/GaAs)^2$.

It remains to notice that $(\tau_f)_{hh} > (\tau_f)_{lh}$ for the DBRT, having a bigger difference at low energies, with respect to that of high energies. Another remarkable distinction is the width of T_2 resonances, which are noticeable widest for lh . This difference yields to a larger confinement for hh inside the embedded QW, with respect to that for lh . Thus greater lifetime for hh in the scattering region is expected.

In Figure 7 the phase time τ_8 and transmission coefficient T_8 , through a superlattice ($n = 8$) undoubtedly

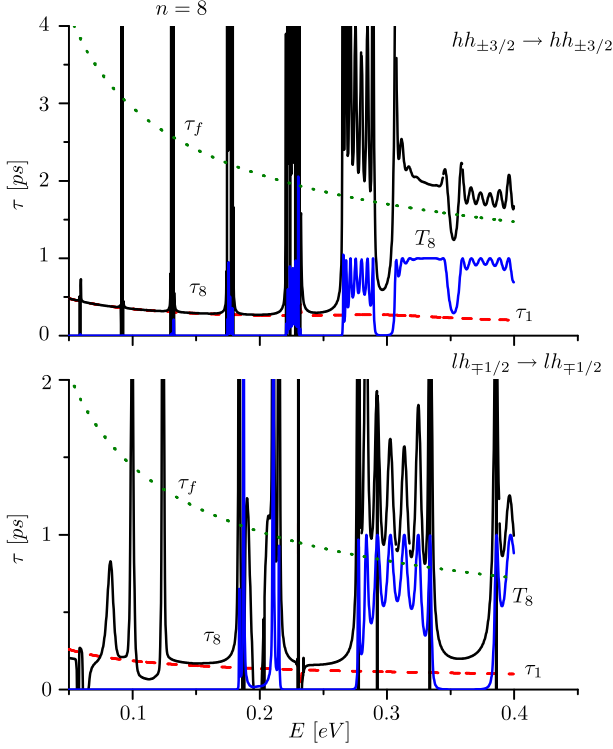


Figure 7: Top(Bottom) panel shows the evolution of the phase time, transmission probability, free motion time through $n = 8$ cells (DBRT) and the phase time through one single cell as function of the incoming energy for direct transitions of $hh_{\pm 3/2}$ ($lh_{\mp 1/2}$). With $V_b = 0.23$ eV, $L_b = 30$ Å and $L_w = 150$ Å. A 30% concentration of Al was fixed inside the barrier.

follow a resonant-mini-band structure. Direct hole transitions were considered and appear indicated in the legends of each panel. For finite periodic systems -which is the case envisioned here-, a finite number of intra-band energy levels [62] are typically observed, at variance with the continuous band structures predicted for infinite periodic systems. In the mini-gaps, T_8 vanishes and τ_8 tends to τ_1 , which is similar to the DBRT case discussed before. On the other hand, in the mini-bands region τ_8 exhibits a resonant behavior approaching τ_f , which behaves as a lower bound [11]. In the scattering regions, τ_8 increases as the incoming energy approximates to any allowed energy level. While, in the forbidden regions the holes propagation is away faster, reflecting the evanescent behavior and the lack of hospitality of the barrier. These evidences for hh and lh phase time, resemble those for electrons as was foretold for the tunneling time in a similar superlattice [11].

Figure 8 exhibits two dissimilar behaviors of τ_{ii} for direct transitions $hh_{\pm 3/2} \rightarrow hh_{\pm 3/2}$ as function of the barrier thickness. For energies under the potential barrier (full triangles) τ_{ii} becomes independent of the barrier thickness, being consistent with Hartman's classical premonition for electrons [29]. In the DBRT, τ_{ii} becomes autonomous starting from $L_b \approx 60$ Å, meanwhile, in a superlattice of $n = 4$ cells, this quantity saturates at about $L_b \approx 50$ Å.

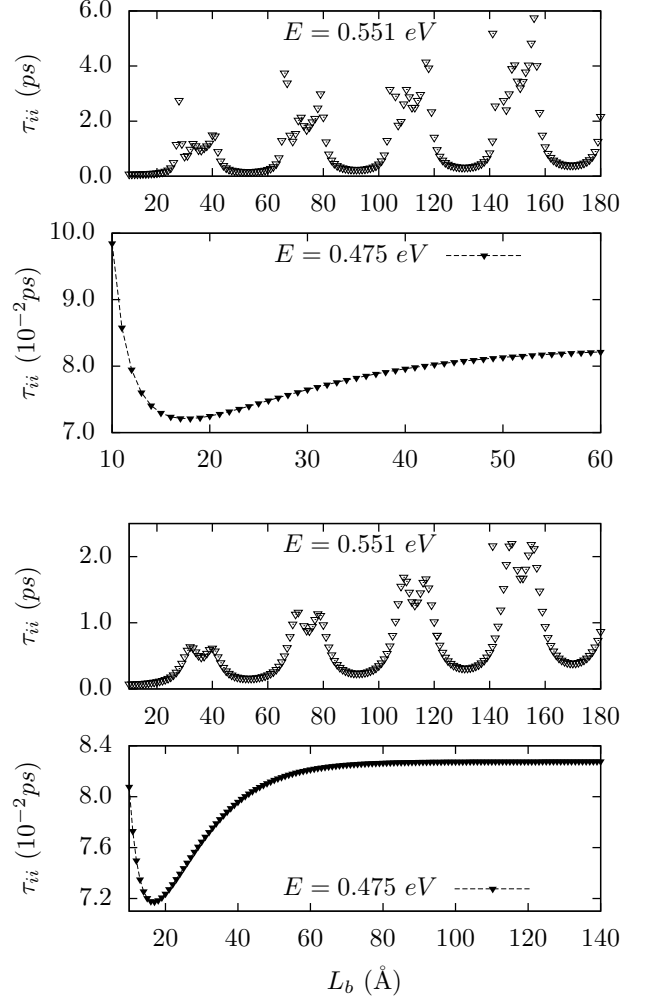


Figure 8: Phase transmission time as a function of the barrier thickness for heavy hole transition $hh_{\pm 3/2} \rightarrow hh_{\pm 3/2}$ within the uncoupled regime, $\kappa_T \approx 0$. Both incident energies E : less (full triangles) and greater (empty triangles) than the barrier height $V_b = 0.498$ eV were fixed at 0.475 eV and 0.551 eV, respectively. The two bottom and top panels represents the numerical values of this time for the DBRT and the superlattice of $n = 4$ cells respectively.

We can also note a decrease of the phase time in the region $(10 - 15)$ Å for the DBRT and around $(10 - 17)$ Å for the superlattice, showing the attractive effect of the barrier, as a reminiscence of the similar behavior widely quoted in the literature for electrons through a simple barrier [8, 9]. For energies higher than the potential barrier (empty triangles) τ_{ii} , in the DBRT and in the superlattice, exhibits a resonant oscillating behavior similar to those of the single barrier (see Figure 4). This is a consequence of an interference effect between the reflected wave and the continuum states, known as Ramsauer-Townsend oscillations as commented above. By comparing Figure 4 and Figure 8, it is clear that oscillations [4, 60] remain robust for the DBRT. The robustness of this feature vanishes for the superlattice, provides that well-resolved oscillating curves are no longer observed for $n = 4$ cells.

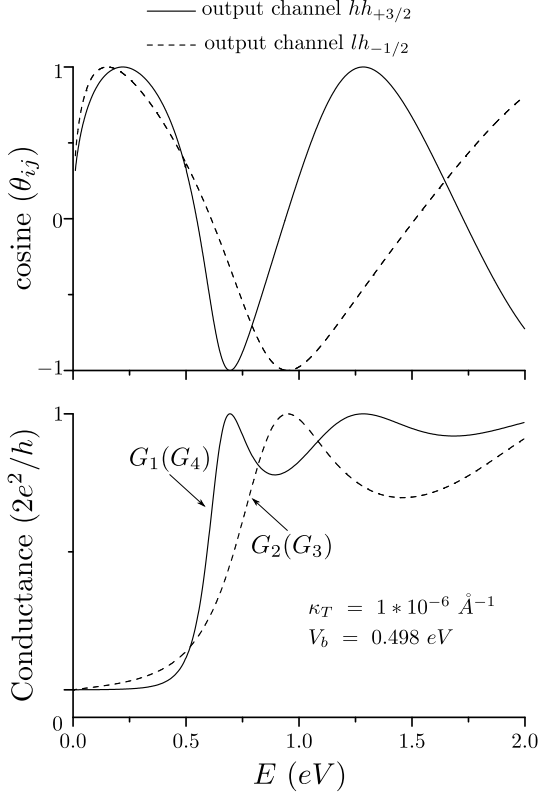


Figure 9: The bottom panel plots the 4 outgoing channel conductances G_j through a single barrier heterostructure with $L_b = 20$ Å, where $i = 1, 4$ (solid line) represents the $hh_{\pm 3/2}$ channels, respectively, and $i = 2, 3$ (dashed line) represents the $lh_{\pm 1/2}$ channels, respectively. The top panel displays the cosine of phase shift for the same transitions.

It is quite well established in the literature the strong relation between the transmission magnitudes and the wave function's phase [17, 19, 62]. Specifically, the giant conductance events are nearly related with phase shifts and phase interference phenomena [19]. It has been shown for various mesoscopic systems, the correlation between the variations of the conductance and an even function of the phase shift, due to an alternatively appearance of maximum-minimum valued sharp peaks or dips, whenever an even functional of the phase shift, changes by almost π radians [17, 19, 54, 55, 63]. Here, the cosine of the phase shift was chosen to verify, whether strike maximum-transmission peaks occur or not, in a negligible conductance background. Commonly, the $\cos(\theta_{ij})$ is plotted, as it is a suitable even function to show evidences of giant conductance events [17, 19].

Figure 9 (bottom panel), presents the conductance G_j to direct channels $hh_{\pm 3/2} \rightarrow hh_{\pm 3/2}$ (solid line), $lh_{\pm 1/2} \rightarrow lh_{\pm 1/2}$ (dashed line), and the cosine of phase shift for the same transitions (top panel) for the uncoupled hole regime as function of the incident energy. It is clear that the maximum values in the conductance for both output channels are always accompanied by an extreme change in the co-

sine of the phase difference. One can see, that the curve for hh output channel (solid line) changes two times in π radians and in the bottom panel appear two G_j maximum correspondingly (at $E \approx 0.72$ eV and at $E \approx 1.25$ eV). Meanwhile for the lh output channel (dashed line), there is only one change (at $E \approx 0.98$ eV). Direct paths contributions are the largest ones, as it follows from vanishing band mixing effects as $\kappa_T \approx 0$. The maximum values shown in the bottom panel of Figure 9, for an even function of $\Delta\theta$ ($\cos\Delta\theta$), at even multiples of π [17, 19, 20, 54, 55], are not enough to confirm an abrupt increment of transmission. Indeed, there is nothing particularly large about hole transmission through a single cell, as that reported for electrons in finite periodic systems with time reversal symmetry [19]. Besides, in the single-cell case, does not exist a resonant mechanism that allows hole conductance to become giant through the barrier. However, it is tempting to have a fairly reference frame to compare to what we will see next for a DBRT. Worthwhile noticing -although not shown here-, the largest contribution of the imaginary scattering amplitude component, that give rise G_j to maximize in the same energy intervals, as we have shown in the Figure 9 bottom panel.

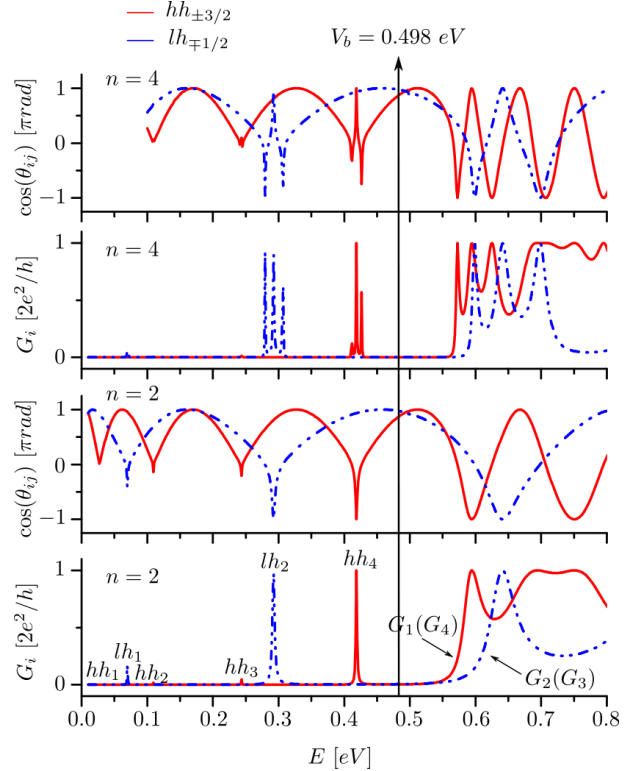


Figure 10: Dependency of the 4 outgoing channels conductance and the cosine of phase shift with hole incident energy, through a DBRT and a superlattice with $n = 4$ cells of width $L_b = 20$ Å, and height $V_b = 0.498$ eV.

Well-established time reversal symmetry of the (4×4) Kohn-Luttinger model, is not fulfilled by the (2×2) subspaces as was recently demonstrated [56]. Events of GG have been observed in many finite periodic systems, which

possess time reversal invariance but as yet not observed in time asymmetric ones. Probably, this explains why other accurate calculations made in the (2×2) Kohn-Luttinger subspaces, did not report GG events for holes [43, 45, 47, 50]. Figure 10 displays the conductance and phase shift behavior as a function of the incident energy, for direct transitions to $hh_{\pm 3/2}$ (solid line) and $lh_{\pm 1/2}$ (dashed line) output channels. The G_i curves exhibit evidences pointing out the existence of well-defined resonances for $E < V_b$. It is relevant in this case, the presence of striking conductance events, as can be clearly noticed in the panels for $n = 2$ of Figure 10. Indeed, peaks lh_2 and hh_4 , have found to have a clear signature of GG phenomenon since: (i) they are sharp resonances, (ii) they keep a simple relation with an even function $\cos(\theta_{ij})_{n=2}$ of the transmission phase $(\theta_{ij})_{n=2}$, thereby peaks' locations at energy, are coincident with those of $(\theta_{ij})_{n=2}$ whenever the last changes by almost π radians in a relative short energy interval [17–19, 23, 62], and finally (iii) there is a strong phase interference mechanism between propagating or evanescent modes, giving rise to resonant transmission [19]. As follows from the scattering theory, the GG mechanism in a DBRT, derives from the interference between states, whenever the incoming modes energy perfectly matches with one of the quasi-stationary states within the embedded QW of the scatterer system. This agreement produces the essential conditions for energy to maximize, *i.e.* a resonant transmission occurs. Sharp peaks become visible at energies $E \cong 0.29$ eV (dashed line) for direct transitions of lh , and for $E \cong 0.42$ eV (solid line) for direct transitions of hh . We have disregarded the lh_1 sharp resonances and others in the low energies region, because they do not reach maximum and also the corresponding phase shifts differ significantly from π radians. In addition, it is necessary to mention the loss of the GG phenomenon in the superlattice. As one can see in the top panels of Figure 10 (for $n = 4$ and $E < V_b$), the $(\theta_{ij})_{n=4}$ changes are not about π radians. In this case the leak of maximum transmission for the superlattice becomes visible. We conjecture the existence of a competitive mechanism when the number of cells grow, and consequently a phase coherence effect rises. For higher energies, the direct G_i might give rise to a *plateau*, and we foretell the probable existence of another related striking feature: the giant resistance. Despite a more ambiguous interference process in this case, a sharp dips are expected as a consequence of a transmission rate decrease, due to a resonant transfer of holes flux toward evanescent modes.

It is likely to underline that the energies of the resonances -whether they are giant or not-, accurately reproduce the quasi-bounded hole spectrum as was published for the DBRT [27], were another approaching frame was applied. This is to say that, none GG phenomenological analysis can possibly be complete if a resonant means is missing. In this sense, to endorse the GG evidences showed in Figure 10, the most immediate tool within the MSA, is the TM technique to estimate the hole states en-

ergies at the QW of the DBRT. The basic idea here, is to search several states of the embedded finite quantum well (fQW), by cautious tuning those of the external infinite quantum well (iQW). The last we had achieved, by imposing that $z_{L,R}$ slowly tends to $z_{1,4}$, respectively (see Figure 11). This method approaches the iQW boundary conditions to those of the fQW, and is a reasonably good sketch for an estimation of some fQW levels.

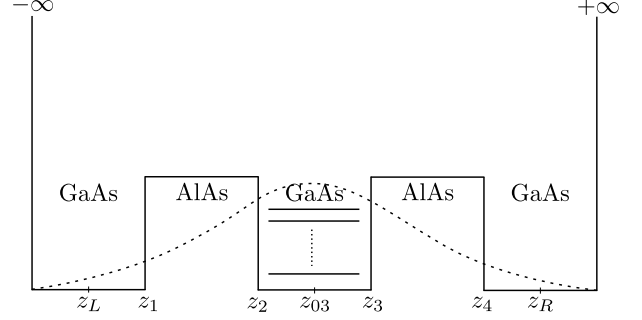


Figure 11: Schematic representation of the quasi-bound-state levels (horizontal lines) and valence band lineup, within an infinite wells quantum well. The ground state wave function (dotted line) is represented qualitatively. The energy is taken as positive for convenience.

Figure 11 shows schematically, holes quasi-bound-state levels (horizontal lines) and valence band lineup, within the iQW. For a numerical estimation of the quasi-stationary levels within the fQW, we consider a cell enclosed between the z_L and z_{03} points. The barriers and well have the same dimensions of the Figure 10. Thus, it is undemanding and straightforward to reproduce a DBRT or a superlattice, by a periodic concatenations of cells from z_{03} [3]. The latter considers facts of equivalence for points $z_1(z_2)$ and $z_3(z_4)$, respectively, as they have the same materials to the left and to the right. As boundary condition for the iQW, is standard to impose the wave function goes to zero at the points $(z_L - \Delta z)$ and $(z_R + \Delta z)$

$$\varphi(z_L - \Delta z) \equiv \varphi(z_R + \Delta z) \equiv 0, \quad (9)$$

being Δz the splitting distance between these points and the infinite potential. In the framework of the TM approach, the latter requirement can be written as:

$$\begin{pmatrix} 0 \\ \varphi'(z) \end{pmatrix}_{(z_R + \Delta z)} = \mathbf{M}_{fd}(z_R + \Delta z, z_L - \Delta z) \begin{pmatrix} 0 \\ \varphi'(z) \end{pmatrix}_{(z_L - \Delta z)}. \quad (10)$$

Therefore, the non trivial solutions of the expression (10) can be numerically determined, by solving the equation

$$\text{Det}\{\mathbf{M}_{AD}(z_R + \Delta z, z_L - \Delta z)\} = 0, \quad (11)$$

being \mathbf{M}_{AD} the *amplitude-derivative* matrix block of the TM \mathbf{M}_{fd} . Up to this end, it is turn clear from Table 2, a reasonably good agreement between our estimation for the energies of several quasi-steady levels of the fQW and

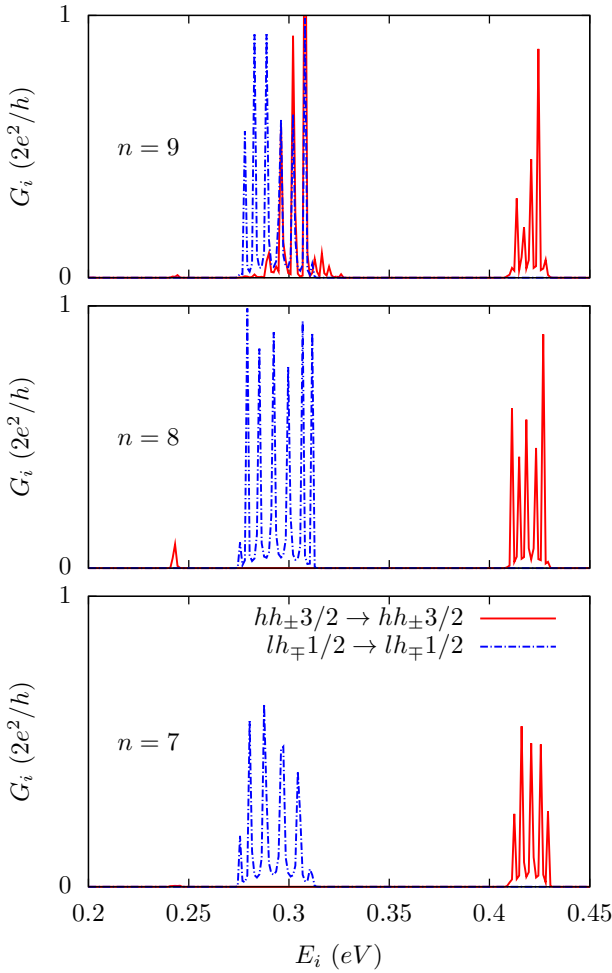


Figure 12: Two-probe conductance through the four direct accessible channels as a function of the incoming energy on the $\kappa_T \approx 0$ limit, for a superlattices of $n = 7, 8, 9$ cells (from bottom to top) in the range of energies between $[0.2 - 0.45]$ eV.

the resonant-band structure displayed in Figure 10. Now it is undoubted, the very existence of these fQW levels, and therefore their role as a fair resonant mechanism of the GG phenomena in the DBRT we claim for. The lh_2 and hh_4 energy values showed here, are a truthful prove of the GG phenomena, predicted for the uncoupled hole transport in the DBRT for sharp resonances allocated at similar energies (see Figure 10).

Figure 12 presents the dependency of the conductance G of hh and lh through a superlattices of $n = 7, 8, 9$ cells with the energy of the incident flux. The holes travel along all four accessible direct channels $hh_{\pm 3/2} \rightarrow hh_{\pm 3/2}$

Table 2: Quasi-steady fQW hole-level for a DBRT structure, quoted by Eq.(11), with $V_b = 0.498$ eV, $L_b = 20$ Å, and $L_w = 50$ Å.

Levels (Labeling from Ref.[45])	Resonances [eV]
hh_2	0.1362
lh_2	0.2978
hh_4	0.4112

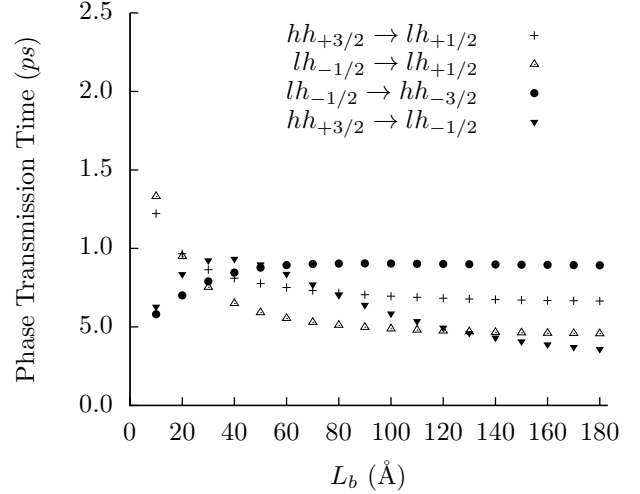


Figure 13: Phase transmission time through one single cell *versus* barrier thickness for the direct and crossed passages of holes in a coupled case ($\kappa_T = 5 \times 10^{-4}$ Å⁻¹) for $E = 0.475$ eV $<$ $V_b = 0.498$ eV.

(solid line) and $lh_{\pm 1/2} \rightarrow lh_{\pm 1/2}$ (dotted-dashed line). It is wide open visible the thinner peaks of the hh resonances, respect to those of the lh ones, since we are restricted on the uncoupled regime and thereby hh -spectrum states are the closest due to their larger effective mass. Further outstanding behavior, is the filter-like effect that can be observed on both flavors of holes in the selected region. Indeed, the barriers become opaque for the hh/lh states at low/high energies, leading to a stronger confinement for the hh/lh at low/high energies. This fact yields a larger/shorter lifetime for hh/lh inside the allowed region of the scatterer system for low energy, at variance with the opposite for higher energies. Dealing with a superlattice of $n = 9$ cells (topmost panel), we found an $hh - lh$ overlap region at the vicinity of 0.3 eV. The phenomenology described in Figure 12, allows us hypothesize it as concerns applications in hole-based electronics, pursuing maximum-minimum conductivity response as function of the charge carrier effective mass.

3.2. Coupled hole regime phenomena

Let us considers first the Hartman effect under this regime. Figure 13 depicts the phase transmission time as a function of the barrier thickness for several crossed transitions paths, namely: $hh_{+3/2} \rightarrow lh_{+1/2}$, $lh_{-1/2} \rightarrow lh_{+1/2}$, $lh_{-1/2} \rightarrow hh_{-3/2}$ and $hh_{+3/2} \rightarrow lh_{-1/2}$, of the sixteen possible ones, through a single-cell scatterer system. This plot shows the phase transmission time curves as a function of the barrier thickness L_b , given fixed $E < V_b$. Notice the changes of τ_{ij} through each path while L_b increases, until τ_{ij} reaches saturation values. This autonomous behavior of the phase time with L_b , unambiguously gives rise to the paradoxical Hartman effect [29], which remains robust, even for a relative strong coupling of holes. Owing to simplicity we dropped the remain transitions, provided they follow a similar tendency. Worthwhile un-

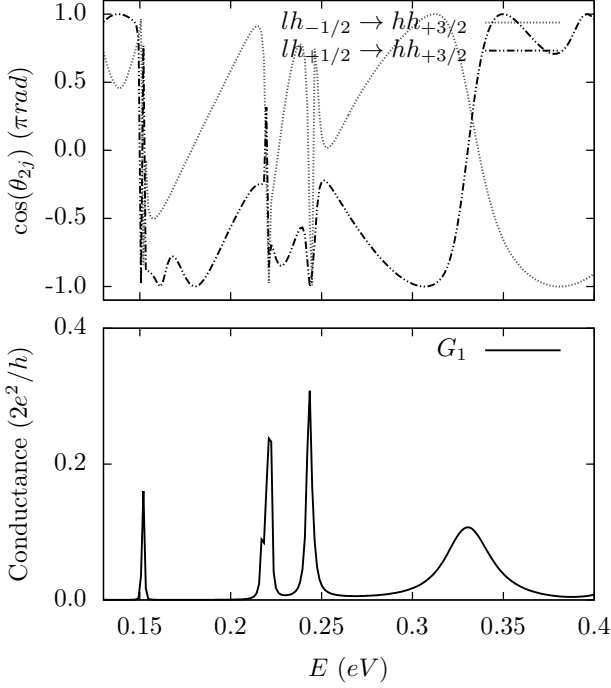


Figure 14: The bottom panel shows the crossed-path contributions to the conductance through the first outgoing channel, G_1 , for a DBRT with barriers of width $L_b = 20$ Å, and height $V_b = 0.498$ eV. The top panel displays the cosine of two phase shifts that match with the same outgoing channel, $hh_{+3/2} \rightarrow lh_{-1/2}$ and $hh_{+3/2} \rightarrow lh_{+1/2}$, both in the same range of energy.

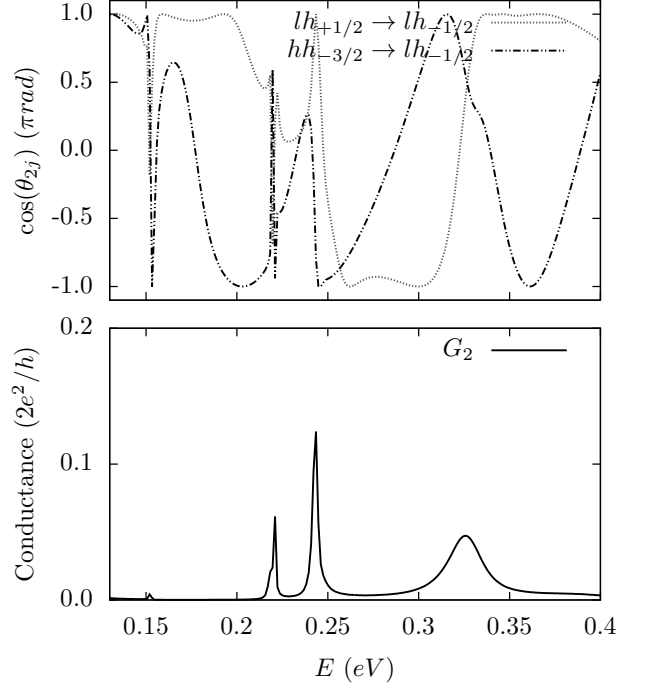


Figure 15: The bottom panel shows the the crossed-path contributions to the conductance through the second outgoing channel, G_2 , for a DBRT with barriers of width $L_b = 20$ Å, and height $V_b = 0.498$ eV. The top panel displays the cosine of two phase shifts that match with the same outgoing channel, $lh_{-1/2} \rightarrow lh_{+1/2}$ and $lh_{-1/2} \rightarrow hh_{-3/2}$, both in the same range of energy.

derlying some characteristics of τ_{ij} transient interval for several paths. Crossed transitions $hh_{+3/2} \rightarrow lh_{+1/2}$ (+) and $lh_{-1/2} \rightarrow lh_{+1/2}$ (up empty triangles), show negative slope before reach saturation. Meanwhile the crossed path $hh_{+3/2} \rightarrow lh_{-1/2}$ (down full triangles), exhibits a double change of slope. These behaviors clearly departs (in the transient interval) from the classical Hartman premonition for electrons and deserve more investigation to shed light on this topic. In the presence of interference effects ($\kappa_T \neq 0$) at $E \approx 0.55$ eV, we have found abrupt tunneling phase changes when $\Delta\theta \approx \pi$ radians, which seems to be an anomalous behavior of the phase time. In Figure 13, we have found an overlap of τ_{ij} for several crossed transitions. For example: with $j : 1(2) \rightarrow 3 : i$ at $L_b \approx 20$ Å, also with $j : 1(2) \rightarrow 2(3) : i$ at $L_b \approx [110, 140]$ Å, and with $j : 1 \rightarrow 2(3) : i$ at $L_b \approx [70, 80]$ Å. In some cases the effective mass changes, and the incoming channels belong to a so called Kramer-up and degenerated hole states [3], while the outgoing channels are Kramer-low ones. It can be readily observed, similar τ_{ij} matches, for other crossed transitions at different values of L_b . These coincidences relate to the strong $hh - lh$ propagating modes mixing, to the simultaneous treatment of the 4-coupled channels of the present approach, and to $hh - lh$ interaction with an effective potential V_{eff} due the barrier broadening. Accordingly, whenever a match in τ_{ij} takes place, the time spent by the hh and lh in the classically forbidden region, shall be the same.

We turn now to discuss how robust are the hole giant conductance features, in the presence of valence-band mixing. Figure 14 and Figure 15 present the conductance and the $\cos(\theta_{ij})_{n=2}$ through the outgoing channels $hh_{+3/2}$ and $lh_{-1/2}$, respectively, as a function of the incoming energy under interference between channels. We had taken $\kappa_T = 10^{-3}$ Å⁻¹. Despite the presence of sharp peaks at $E < V_b$ (qualitatively similar to those showed in Figure 10), as one can observe at $E \cong 0.16$ eV, $E \cong 0.22$ eV and $E \cong 0.24$ eV in Fig.14, it is not seen a neat concordance with the widely accepted GG formulation posted above [17, 19, 54, 55, 63], and illustrated in Fig.10. Firstly there is not a nice correspondence between the highest peak of G_1 at the vicinity of $E = 0.24$ eV (see Fig.14 bottom panel) and the fluctuation of $(\theta_{ij})_{n=2}$, which for this peak is sensitive less than π radians (see Fig.14 top panel). On the other hand, the values of $G_{1,2}$ exhibited in Fig.14 and Fig.15, respectively, are in average almost one order smaller than those shown by Fig.10, being the comparative behavior observed in Fig.15 even more restrictive in this sense, with respect to Fig.10. Following these evidences, we conjecture so far, that the GG events are not straightforward signatures for hole tunneling traversing a DBRT, under a selected range of parameters in the coupled-particle regime.

Additional remarkable differences become clear from a comparison of this trend in the coupled hole regime and Figure 10. For instance, there is a small shift between

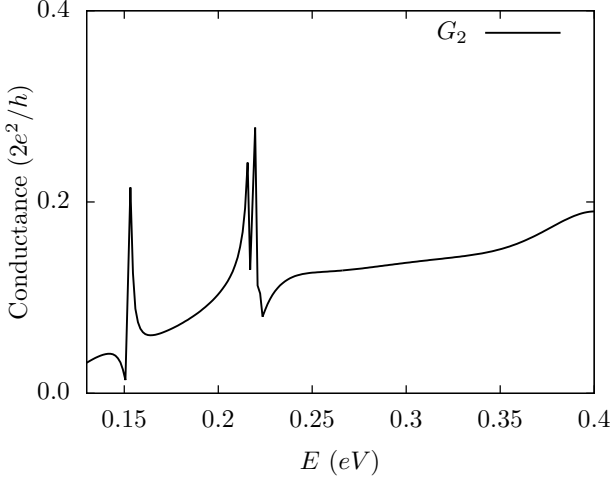


Figure 16: Full contributions to the conductance through the second outgoing channel, G_2 , for a DBRT with barriers of width $L_b = 20$ Å, and height $V_b = 0.498$ eV.

the position in energies of the peaks and the changes in the $\cos(\theta_{ij})_{n=2}$. We guess that the last reflects the loss of maximum transmission when the valence-band mixing, *i.e.* the interference between paths is incremented. Besides, the G_n oscillations spectra in the low-energy interval shown in Fig.15, seem to be of the Fano-type leading to assume the existence of interference of embedded-QW discrete levels with a continuum. The later gives rise to characteristically asymmetric peaks in transmission spectra [64].

The porpoise of Figure 17, is to briefly analyze further anomalous features in the transmission phase time spectra. Fig.17 displays in panel (a) the $\cos(\theta_{ij})_{n=1}$ for the crossed $lh - hh$ transition $lh_{+1/2} \rightarrow hh_{-3/2}$ (dashed line, $i : 3 \rightarrow 4 : j$). In panel (a) with dotted line, we plot the difference of the the same magnitude for the path $i : 3 \rightarrow 3 : j$ with respect to the path $i : 3 \rightarrow 4 : j$. The bottom panel (b) plots tunneling phase time for the crossed-transition $i : 3 \rightarrow 4 : j$ through a single barrier heterostructure. In the presence of interference effects ($\kappa_T \neq 0$) at $E \approx 0.55$ eV, the phase changes abruptly when $\Delta\theta \approx \pi$ radians, as can be seen from the dashed line in the top panel of Figure 17. Both curve in panel (a) show a clear correspondence of abrupt changes in $\cos\theta_{ij}$ with observed peaks(dips) of τ_{ij} , which seem to be an anomalous behavior of the phase time, as they resemble Fano-like resonances due theirs asymmetry hallmark [64]. In the neighborhood of 0.8 eV [see panel (b)] we have found Fano-like positive (negative) peaks (dips) of τ_{ij} with $i \neq j$, displayed in the bottom panel of Figure 17. They are associated with changes of the phase in almost $\pi/2(\pi/3)$ radians, and are plotted in the top panel with dashed line. We also have observed, although will not be shown here, local increments of transmission coefficients in the energy vicinity, where negative dips appeared, though regretfully they need more investigation to derive proper conclusions.

Most interestingly, though, we found indications that

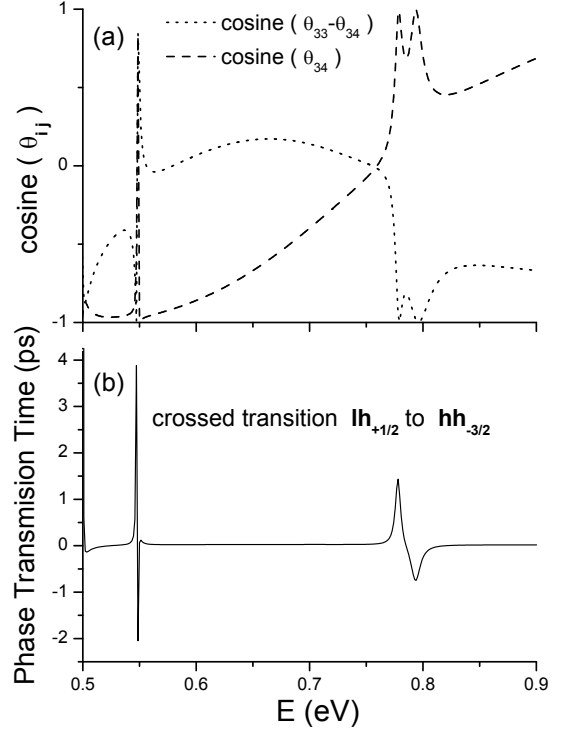


Figure 17: The bottom panel plots tunneling phase time for the crossed-transition $j : 3 \rightarrow 4 : i$ through a single barrier heterostructure at $\kappa_T = 0.001$ Å⁻¹, with $L_b = 20$ Å and $V_b = 0.498$ eV. Top panel shows the cosine of phase shift for the same transition $j : 3 \rightarrow 4 : i$ (dashed line) where the first number stands for the input channel j and the other stands for the output one i . In dotted line the same magnitude is shown for the direct path $j : 3 \rightarrow 3 : i$ with respect to the crossed path $j : 3 \rightarrow 4 : i$.

might be connected to possible giant conductance events in the single-cell case, which we omit graphically here because of brevity. There were found two prompt shifts in transmission phase amplitude, equivalent to an even multiple of π ($|\Delta\theta_{ij}| = 6\pi$) at $\kappa_T \approx 0.01$ Å⁻¹, similar to those plotted in Figure 10. One of them, appear in $lh_{+1/2} \rightarrow lh_{-1/2}$ intra-band transition ($i : 3 \rightarrow 2 : j$) when L_b varies within $[10 - 20]$ Å range. The second one, was observed through $hh_{-3/2} \rightarrow lh_{+1/2}$ inter-band transition ($i : 1 \rightarrow 4 : j$) when L_b varies within $[120 - 130]$ Å range. Then, maxima of G_j could be expected for those crossed paths, not only varying the incident energy, but the barrier thickness as well. However, a clear resonant mechanism in this case remains a puzzle and further investigations need to be addressed to clarify wether the effect of giant conductance for holes, is expected to arise under valence-band coupling phenomena during transport trough a single-cell system.

4. Concluding Remarks

Relevant and striking quantum transport features of holes, directly connected to the phase, the phase shift and the phase resonant interference phenomena are: the giant conductance-resistance events, the Hartman effect, and the earlier phase propagation in the barrier. Several results nicely resemble those previously reported for electrons [11], while some predictions of the MSA model are in acceptable qualitative compliance with the experiments [2, 48, 53] and with theoretical predictions [46, 62]. Theoretical evidences of the giant conductance phenomena for decoupled hole transmission through DBRT were exhibited. In this case a trustworthy resonant mechanism supporting this anomaly, is the alignment of the incident propagation energy with one of the quasi-bond hole states of the embedded quantum well in the DBRT. This mechanism was confirmed with an independent numerical calculations of several quasi-bound levels. The giant conductance effect vanishes in the presence of valence-band particles coupling and by tuning the number of superlattice layers as well. The hole phase transmission time for a $(GaAs/Al_{0.3}Ga_{0.7}As/GaAs)^n$ superlattice, shows a resonant mini-bands structure in the scattering regions, having the free motion as an inferior limit time. Moreover, in the forbidden regions the holes propagation became away faster and was shown τ_{ii} to be inferiorly bounded by the single-cell phase time τ_1 . In the DBRT mini-gaps regions, τ_{ii} moves forward from the free motion time, suggesting a more speedily phase propagation within the barrier. The Hartman's classic prediction is observed robust for null and finite hole band mixing. Was presented an alternate-selective confinement strength independently for both flavors of holes, implying filter-like effects on the effective mass *via* the manipulation of the incident energy in the uncoupled hole regime.

Acknowledgments

We thanks Dr. H. Rodríguez-Coppola for clue suggestions in some numerical treatments. One of the authors (L.D-C) gratefully acknowledges the Visiting Academic Program of the UIA/México and the facilities of the IFSC-USP/São Carlos, Brasil.

References

- [1] H. Schneider, H. T. Grahn, K. Klitzing, and K. Ploog, Phys. Rev. B **40**, 10040 (1989).
- [2] D. Dragoman and M. Dragoman, J. Appl. Phys. **93**, 6133 (2003).
- [3] L. Diago-Cisneros, H. Rodríguez-Coppola, R. Pérez-Álvarez, and P. Pereyra, Phys. Rev. B **74**, 045308 (2006).
- [4] L. Diago-Cisneros, H. Rodríguez-Coppola, R. Pérez-Álvarez and P. Pereyra, Rev. Mex. Fís **53**, 7 (2007).
- [5] P. Pereyra and H. Simanjutak, Phys. Rev. E **75**, 1 (2007).
- [6] H. G. Winful, Phys. Rev. Lett **91**, 26 (2003).
- [7] H. G. Winful, Phys. Rev. Lett **90**, 2 (2003).
- [8] E. H. Hauge and J. A. Støvneng, Rev. Mod. Phys **61**, 917 (1989).
- [9] R. Landauer and Th. Martin, Rev. Mod. Phys **66**, 217 (1994).
- [10] P. Pereyra, V. G. Ibarra-Sierra and J. L. Cardoso, Microelectronics Journal **40**, 779 (2009).
- [11] P. Pereyra, Phys. Rev. Lett. **84**, 1772 (2000).
- [12] A. M. Steinberg, P. G. Kwiat and R. Y. Chiao, Phys. Rev. Lett **71**, 708 (1993).
- [13] Ch. Spielmann, R. Szipöcs, A. Stingl, and F. Krausz, Phys. Rev. Lett. **73**, 2308 (1994).
- [14] S. Chu and S. Wong, Phys. Rev. Lett **48**, 738 (1982).
- [15] S. Bosanac, Phys. Rev. A **28**, 557 (1983).
- [16] A. B. Shvartsburg, M. Marklund, G. Brodin and L. Stenflo, Phys. Rev. E **78**, 016601 (2008).
- [17] A. Kadigrobov, A. Lagoskin, R. I. Shekter and M. Jonson, Phys. Rev. B **52**, R8662 (1995).
- [18] A. Kadigrobov and M. Jonson, Applied Physics Report **94**, 6 (1994).
- [19] P. Pereyra, Physica E **17**, 209 (2003).
- [20] N. K. Allsopp, J. Sánchez-Cañizares, R. Raimondi and C. G. Lambert, J. Phys. Condens. Matter **8**, L377 (1996).
- [21] Roberto Romo, Phys. Rev. B **66**, 245311 (2002).
- [22] Jorge Villavicencio and Roberto Romo, Phys. Rev. B **68**, 153311 (2003).
- [23] Junling Wu, Baigeng Wang, Jian Wang and Hong Guo, Phys. Rev. B **72**, 195324 (2005).
- [24] Yuanbo Zhang, Victor W. Brar, Feng Wang, Caglar Girit, Yossi Yayon, Melissa Panlasigui, Alex Zettl and Michael F. Crommie, Nature Physics **4**, 627 (2008).
- [25] A. K. Geim and K. S. Novoselov, Nature Materials **6**, 183 (2007).
- [26] Guangyu Xu, Carlos M. Torres Jr., Emil B. Song, Jianshi Tang, Jingwei Bai, Xiangfeng Duan, Yuegang Zhang and Kang L. Wang, arXiv.org (to appear in Nano Letters) (2010).
- [27] R. Wessel and M. Altarelli, Phys. Rev. B **39**, 12802 (1989).
- [28] E. P. Wigner, Phys. Rev. **98**, 145 (1955).
- [29] T. E. Hartman, J. Appl. Phys **33**, 12 (1962).
- [30] L. A. MacColl, Phys. Rev **40**, 621 (1932).
- [31] D. Bohm, *Quantum Theory*, (Prentice-Hall, New York, 1951).
- [32] F. T. Smith, Phys. Rev. **118**, 349 (1960).
- [33] A.I. Baz', Sov. J. Nucl.Phys. **4**, 182 (1967).
- [34] M. Büttiker and R. Landauer, Phys. Rev. Lett. **49**, 1739 (1982).
- [35] M. Büttiker Phys. Rev. B **27**, 6178 (1983).
- [36] G. Nimtz, A. Haibel, and R.-M. Vetter, Phys. Rev. E **66**, 037602 (2002).
- [37] A. Ranfagni, D. Mugnai, P. Fabeni and G. P. Pazzi, Appl. Phys. Lett. **58**, 774 (1991).
- [38] A. Enders and G. Nimtz, J. Phys. France **12**, 1693 (1992).
- [39] J. M. Lüttinger and W. Kohn, Phys. Rev. **97**, 869 (1955).
- [40] L. Diago-Cisneros, *Tunelaje multicanal y simetrías de los huecos en heteroestructuras semiconductoras*, Universidad de La Habana, Facultad de Física, La Habana (2005).
- [41] P. A. Mello, P. Pereyra and N. Kumar, Ann. Phys. (N.Y) **181**, 290 (1988).
- [42] J. Imry and R. Landauer, Rev. Mod. Phys. **71**, 306 (1999).
- [43] A. P. Heberle, X. Q. Zhou, A. Tackeuchi, W. W. Rühle, and K. Köhler, Semicond. Sci. Technol. **9**, 519 (1994).
- [44] T. Kumar, M.Cahay, and K. Roenker, Phys. Rev. B **56**, 4836(1997).
- [45] G. Klimeck, R. Chris Bowen, and T. B. Boykin, Supperlattices and Microstructures **29**, 188 (2001).
- [46] R. Landauer, Nature (London) **341**, 567 (1989).
- [47] M. F. Krol, S. Ten, B. P. McGinnis, M. J. Hauduk, G. Khitrova, and N. Peyghambarian, Phys. Rev. B **52**, R14344 (1995).
- [48] S. Ten, M. F. Krol, P. T. Guerreiro, and N. Peyghambarian, Appl. Phys. Lett. **69**, 3387 (1996).
- [49] M. Morifuji and C. Hamaguchi, Phys. Rev. B **52**, 14131 (1995).
- [50] M. U. Erdogan, K. W. Kim, and M. A. Stroschio, App. Phys. Lett. **62**, 1423 (1993).
- [51] A. D. Sánchez and C. R. Proetto, J. Phys. Condens. Matter **7**, 2059 (1995).

- [52] K. V. Rosseau, K. L. Wang, and J. N. Schulman, Superlattices and Microstructures **6**, 67 (1989).
- [53] E. E. Mendez, W. I. Wang, B. Rico, and L. Esaki, Appl. Phys. Lett **47**, 415 (1985).
- [54] P. G. N. de Vegvar, T. A. Fulton, W. H. Mallison, and R. E. Miller, Phys. Rev. Lett. **73**, 1416 (1994).
- [55] H. Pothier, S. Guéron, D. Esteve, and M. H. Devoret, Phys. Rev. Lett. **73**, 2488 (1994).
- [56] L. Diago-Cisneros, H. Rodríguez-Coppola, R. Pérez-Alvarez, and P. Pereyra, Phys. Scripta **71**, 1 (2005).
- [57] G. Nimtz, *Proceedings of the Adriatic Research Conference on Tunneling and its implications*, pp.223 (ICTP, Trieste, Italy, 1996).
- [58] A. M. Steinberg and R. Y. Chiao, Phys. Rev. A **49**, 3283 (1994).
- [59] We have obtained the amplitude of the exponential fitting function, for the phase transmission time with different sections of barrier thickness, to be constant starting from 55 Å.
- [60] Luis de la Peña, *Introducción a la Mecánica Cuántica*, Universidad Nacional Autónoma de México, Fondo de Cultura Económica, 2006, Cap.6.
- [61] In additions of an exponential growing functions, adjustments *via* n -order polynomial (with $n = 3, 4$) and cycloid functions are suitable as well.
- [62] P. Pereyra and E. Castillo, Phys. Rev. B **65**, 205120 (2002).
- [63] V. T. Petrashov, V. N. Antonov, P. Delsing and R. Claeson, Phys. Rev. Lett **70**, 3 (1993).
- [64] U. Fano, Phys. Rev. **124**, 1866 (1961).